Numerical simulation for optimising of inlet and outlet positions for mechanical ventilation and heat dissipation - A case study to improve ventilation in an indoor 110kV substation

Haomai Zhang[1], Ling Wang[1], Peng Yang[1*], Yingwen Liu[1*], Chao Zhu[2], Lv Wang[2], Hua Zhong[3]
1 Key Laboratory of Thermo-Fluid Science and Engineering of MOE, School of Energy and Power Engineering, Xi'an Jiaotong University, Xi'an 710049, China;
2 State Grid Shaanxi Electric Power Research Institute, Xi'an, 710000, China
3 London South Bank University, UK, SE1 0AA

Abstract: Efficient ventilation and heat dissipation in indoor substations are crucial for the stable operation of transformers. This study investigates the impact of inlet and outlet positions on ventilation and heat dissipation performance in a 110kV indoor substation using computational fluid dynamics. A model of the 110kV main transformer chamber is developed. Twelve combinations of inlet and outlet positions are analysed. Inlet positions include side walls parallel to radiators, side walls perpendicular to radiators and both side walls perpendicular to radiators. Outlet positions include the top of the chamber, the side of the inlet, adjacent to the inlet, and opposite inlet. Results demonstrate that locating outlets at the top of the chamber reduces transformer temperature by 0.5-1.6℃ and increases energy utilization by 8.6%-24.8% regardless of inlet position. Two opposite inlets perpendicular to radiators allows even air distribution between radiators. And this configuration reduces transformer temperature by 3.4℃ when the outlet is located at the top of the chamber. Overall, the optimal ventilation design involves top chamber outlets and inlets on opposite walls perpendicular to radiators.

Keywords: Indoor substation ventilation; Inlet and outlet positions; Computational fluid dynamics; Heat dissipation; Transformer cooling

*Corresponding author. Email address: ywliu@mail.xjtu.edu.cn and yp2019@mail.xjtu.edu.cn

1 Introduction

Efficient ventilation and heat dissipation are critical in electrical substations to ensure stable operation and prevent equipment overheating. With increasing transformer loads, indoor forced-air ventilation is often utilized for cooling in substations. Optimizing the design of ventilation systems is thus an important consideration for indoor substation performance. This study aims to improve indoor substation ventilation and heat dissipation capacity through numerical analysis of different inlet and outlet configurations in a 110kV indoor substation.

Previous researchers have studied the ventilation and heat dissipation of indoor substations. Xie et al. [1] analysed the influences of ventilation quantity, location, and size of the inlet and outlet on ventilation and heat dissipation. Liu et al. [2] developed a new ventilation optimisation method based on the variational method to solve ventilation and heat transfer problems. Xu and Zou [3] proposed a fast computational fluid dynamics (FFD) method to establish a substation model and verified that this method can effectively represent the flow and heat dissipation characteristics of the substation. Liu et al. [4] studied the influence of the installation positions of fans in the main transformer chamber on the heat dissipation effect of the transformer. Xu et al. [5] studied the influence of the size of the inlet and outlet on indoor ventilation. Cheng et al. [6] established a simulation model of the electromagnetic, thermal, and flow fields of a transformer and analysed the influence of the box-in structure on the temperature rise of

the transformer and its surrounding environment under different ambient wind speeds. Wei et al. [7] proposed a simulation device suitable for the experiment of a split cooling device. Sometimes underground substations are built to save space. A. Bidarmaghz et al. [8] proposed a cooling method for an underground substation that uses a heat pump to absorb the heat in the substation and release it into the tunnel through a heat exchanger. Peng et al. [9] simulated outdoor transformers with noise barriers and studied the effect of barriers on heat dissipation. Perng et al. [10] established a multi-objective particle swarm optimiser for optimal inlet size and reduced noise and power consumption.

Furthermore, previous researchers have studied ventilation and heat dissipation in other buildings. S. Wiriyasart and P. Naphon [11] used CFD to analyse the effects of unilateral and central air inlets on air and temperature distribution in a multi-heat source workshop. Zheng et al. [12] studied the performance of an air conditioning system with two air supply modes for a simplified office room through numerical simulation and physical experimentation. Chen [13] compared the ventilation performance of four different air supply devices in an office environment by numerical simulation. Chen [14] studied the effect of fan installation positions on the ventilation of a signal base station. He et al. [15] studied the ventilation performance of residential buildings, and the results showed that the design of roof window and door openings, indoor space geometry and climate conditions had a significant impact on indoor ventilation performance. L. Tong et al. [16] developed a flow-guide device for adjusting the pressure distribution of duct branches and conducted a full-scale test for a central exhaust system installed with the flow-guide devices referring to a factory workshop with 30 heat and contaminant sources, which showed that ventilation performance improved significantly. A. Staveckis and A. Borodinecs [17] studied impinging jet ventilation, and the results show that the circular opening provides large contaminant removal and air exchange effectiveness. Huang et al. [18] numerically investigated the effects of ventilation duct number and duct geometry on duct ventilation performance in a subway tunnel. Huang et al. [19] investigated different ventilation strategies to find a ventilation method with high performance in a subway tunnel, and their results showed that the combined ventilation ducts and partitioning blocks installed along the middle of the tunnel are helpful for air exchange. J. Park et al. [20] used six different geometries of ventilation ducts to optimise the design for better air quality.

Previous research has explored numerous factors influencing ventilation performance in indoor substations, including inlet/outlet sizes, fan positions, and outdoor conditions. However, most studies have not considered the impact of relative inlet and outlet locations on air distribution, which is critical for heat dissipation. This represents a gap in knowledge regarding optimal ventilation design for indoor substations. This study aims to address this gap by proposing energy utilisation coefficient and surface transfer coefficients as new parameters to evaluate variable ventilation effects. Through computational fluid dynamics (CFD) analysis of a 110kV substation under different inlet/outlet configurations, the work identifies an optimal layout to maximize ventilation and cooling.

2. Physical model

The indoor substation simulation model was constructed according to the actual indoor substation building form. **Fig. 1** shows the model of the main transformer chamber. The transformer is located in the middle of the room. The height between the bottom of the transformer and the ground is 0.48m. Sixteen

sets of radiators are on both sides of the main transformer. The outlet is located 9 m from the bottom of the main transformer chamber. Three outlets are placed separately, and the distance between each outlet is 1.2 m. An exhaust fan is placed at each outlet. **Tab. 1** shows the information of the fan. The dimensions of each component are marked in **Fig. 1**.

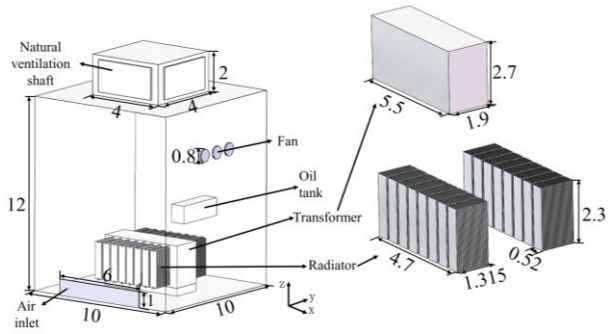

Tab. 1 Information of the fan

Type	Axial fan
Diameter	800 mm
Air volume	17670 $m^3 \cdot h^{-1}$
Total pressure	277 Pa
Rotational speed	1450 $r \cdot min^{-1}$

Fig. 1. Model of the main transformer chamber

In this paper, three types of air intake layout schemes are designed. **Fig. 2** illustrates that in scheme 1, the air inlet is located at the central bottom of the wall and is parallel to the plane where the radiator is located. In scheme 2, the air inlet is located at the central bottom of the wall and is perpendicular to the plane where the radiator is located. In scheme 3, the air inlet is located at the central bottom of the two opposite walls and is perpendicular to the plane where the radiator is located. Based on each air inlet scheme, the exhaust outlet has four position scenarios, which are at the top of the main transformer chamber (Scenario A), on the same side of the inlet (Scenario B), adjacent to the inlet (Scenario C), and opposite to the inlet (Scenario D).

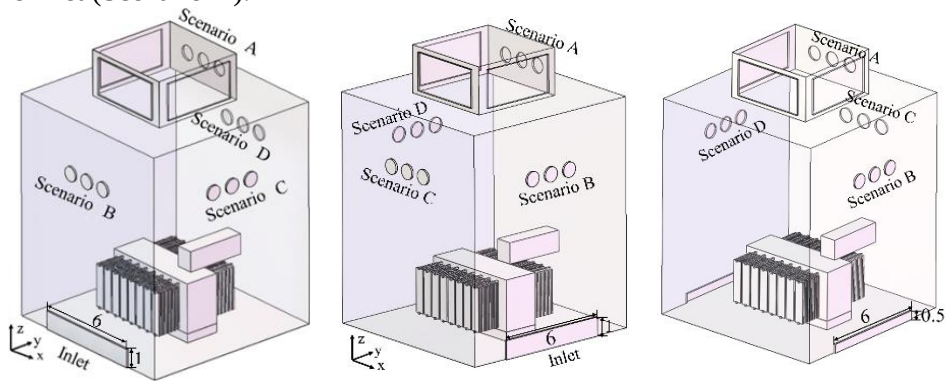

(a) Scheme 1 (b) Scheme 2 (c) Scheme 3

Fig. 2. The models of three inlet schemes and four outlet scenarios of each inlet scheme

3. The numerical method

3.1. Governing equations

A three-dimensional model was used to analyse the temperature and flow fields in the main transformer chamber. Although the process of airflow and heat transfer in the room is overly complicated, it satisfies the continuity, momentum, and energy equations [12]. These governing equations are given by:

$$\nabla \cdot (\rho \vec{V}) = 0 \quad (1)$$

$$\nabla \cdot (\rho \vec{V}\vec{V}) = -\nabla p + \nabla \vec{\tau} + \rho \vec{g} \quad (2)$$

$$\nabla\cdot(\rho T\vec{V}) = \nabla\cdot(\frac{\lambda}{c_p}\mathrm{grad}T)) + S_T \tag{3}$$

where ρ is the density, kg·m^{-3}, $\vec{V}$ is the velocity vector, m·s^{-1}, τ is the viscous force, Pa, T is the thermodynamic temperature, K, λ is the thermal conductivity, W·m^{-1}·K^{-1}, S_T is the source term, W·m^{-3}.

In this paper, the turbulence problem of airflow in the main transformer chamber is solved by the Realizable k-ε model [22]. The governing equations of turbulent kinetic energy k and dissipation rate ε are shown in equations (4) and (5) :

$$\frac{\partial}{\partial x_j}\left(\rho\kappa u_j\right) = \frac{\partial}{\partial x_j}\left[\left(\mu + \frac{\mu_t}{\sigma_k}\right)\frac{\partial\kappa}{\partial x_j}\right] + G_k + G_b - \rho\varepsilon - Y_M \tag{4}$$

$$\frac{\partial\left(\rho\varepsilon u_i\right)}{\partial x_i} = \frac{\partial}{\partial x_j}\left[\left(\mu + \frac{\mu_t}{\sigma_\varepsilon}\right)\frac{\partial\varepsilon}{\partial x_j}\right] + C_1\rho S\varepsilon + C_{1\varepsilon}\frac{\varepsilon}{\kappa}C_{3\varepsilon}G_b - C_{2\varepsilon}\rho\frac{\varepsilon^2}{k+\sqrt{\nu\varepsilon}} \tag{5}$$

The values of the model constants $C_{1\varepsilon}$, $C_{2\varepsilon}$, $C_{3\varepsilon}$, σ_k and σ_ε are derived from basic turbulence experiments and have the following default values:$C_{1\varepsilon}$ is 1.44, $C_{2\varepsilon}$ is 1.9, $C_{3\varepsilon}$ is 1.3, σ_k is 1.0; σ_ε is 1.2 [22].

In this paper, considering the radiation between the transformer and radiators and the wall, the discrete coordinate method (DOM) is used to solve the radiation transfer equation in STAR CCM+ [23]. The radiation transfer equation (RTE) is as follows:

$$\frac{\mathrm{d}I_\lambda}{\mathrm{d}s} = -\beta_\lambda I_\lambda + k_{a\lambda}I_{b\lambda} + \frac{k_{s\lambda}}{4\pi}\int_{4\pi} I_\lambda\Omega\mathrm{d}\Omega + k_{pa\lambda}I_{pb\lambda} + \frac{k_{ps\lambda}}{4\pi}\int_{4\pi} I_\lambda\Omega\mathrm{d}\Omega \tag{6}$$

where I_λ is radiation intensity, W·m^{-3}; $I_{b\lambda}$ is blackbody intensity, W·m^{-3}; s is the distance in the direction, m; $k_{a\lambda}$ and $k_{s\lambda}$ are absorption coefficient and scattering coefficient; $k_{pa\lambda}$ and $k_{ps\lambda}$ are particle absorption coefficient and particle scattering coefficient, respectively. Ω is the solid angle, sr.

3.2. Boundary conditions

The Boussinesq hypothesis is used to consider the effect of buoyancy. The acceleration of gravity in the z direction is -9.81 m·s^{-2}. The thermophysical properties of air at 30℃ are shown in **Tab. 2**. The material of the main transformer and chip radiator is aluminium. In this study, the oil flow in the transformer and radiator is ignored, and the oil flow in the transformer is equivalent to solid heat conduction. Therefore, the thermal conductivity inside the solid at this time is the equivalent thermal conductivity.

Tab. 2 Thermophysical properties of air at 30℃

Physical property	Value
Density	1.165 kg·m^{-3}
Thermal conductivity	0.267 W·m^{-1}·K^{-1}
Specific heat capacity	1005 J·kg^{-1}·K^{-1}
Dynamic viscosity	1.86×10^{-5} kg·m^{-1}·s^{-1}
Coefficient of thermal	3.3×10^{-3} K^{-1}

Tab. 3 Physical properties of aluminium

Physical property	Value
Density	2702 kg·m^{-3}
Equivalent thermal conductivity	5000 W·m^{-1}·K^{-1}
Specific heat capacity	903 J·kg^{-1}·K^{-1}

The outlets are provided with fans and the fan is simplified into the velocity boundary. The heat flux on the top surface of the transformer is calculated according to **Tab. 4** and equation (7). In equation (7), Q is heating power, kW; P_0 is no-load loss, kW; β is load rate, the value in this paper is 1, P_k is load-loss, kW, A is the area of the transformer top surface, m^2. The boundary conditions are shown in **Tab. 5**.

Tab.4 Parameters of the main transformer

Parameter	Value
No-load loss	24.85kW
Load loss	180.94kW
Area of top surface	10.45m^2

$$q = \frac{Q}{A} = 1000\frac{P_0 + \beta^2 P_k}{A} \quad (7)$$

Tab. 5 Boundary condition setting

Name	Type	Value
Inlet	Pressure inlet	Reference pressure: 0Pa Temperature: 30℃ Area: 6m^2
Outlet	Velocity outlet	-9.7 m/s (The - indicates that air flows out of the chamber.)
Top surface of the transformer	Heat flux	19692.82 W·m^{-2}
Surface of the chamber	Wall	Adiabatic
Surface of the radiator and transformer	Wall	Coupling

3.3. Grid independence

In this study, meshing is performed in STAR CCM+. To reduce the number of grids and improve computing efficiency, the cutting body mesh model is selected when the mesh is divided, and the radiator area grid is locally encrypted (As shown in **Fig.3 (a)**). As can be seen from **Fig. 3 (b)**, most of the mesh quality is maintained between 0.1-1, indicating that the mesh quality is good. **Fig. 3 (c)** shows that the maximum temperature of the main transformer varies with the number of grids. With the gradual increase in the number of grids, the maximum temperature of the main transformer first increases and then tends to stabilise. Therefore, a grid of 3.8 million is used to conduct the following simulation calculations.

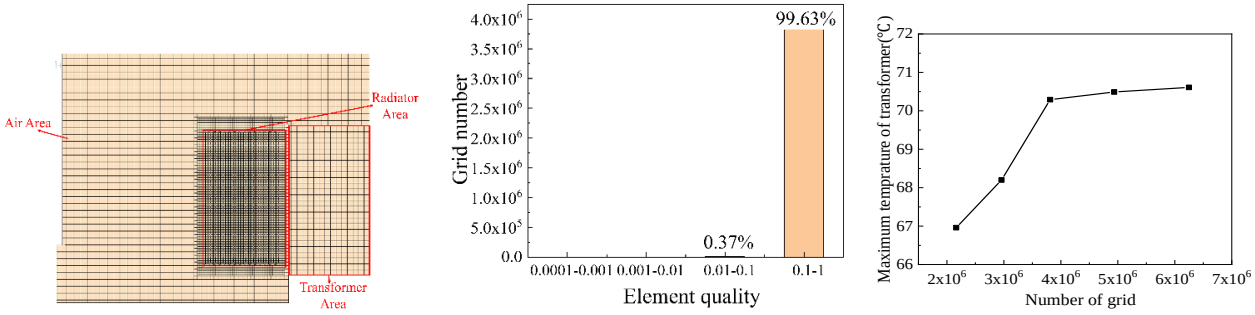

a. Grid diagram b. Mesh quality c. Grid independence verification

Fig. 3. Grid introduction

4 Verification of model and numerical method

In this paper, the accuracy and feasibility of the numerical method are verified by the model of a 110 kV mechanical ventilation substation with the existing test data. The layout of indoor wind speed and temperature measurement points is as follows:

One test point is placed at the inlet in each of the four corners of the main transformer chamber. The test points are located at the geometric centre of the inlet, and the distance from the inlet plane is 0.2 m.

Six test points are arranged around the main transformer. When the height of the test points is 0 m, the test points near the radiators are arranged at the bottom of the radiators, and the other test points are all 1 m away from the main transformer surface; When the height of the points is 1 m and 2 m all the test points are 1 m away from the main transformer surface and radiator surface. **Fig. 4** shows pictures of spot test points. **Tab.6** shows the test instrument introduction. The measurement process lasts for 10 minutes, and the instrument can collect data every 5 s. The final wind speed and temperature are average values.

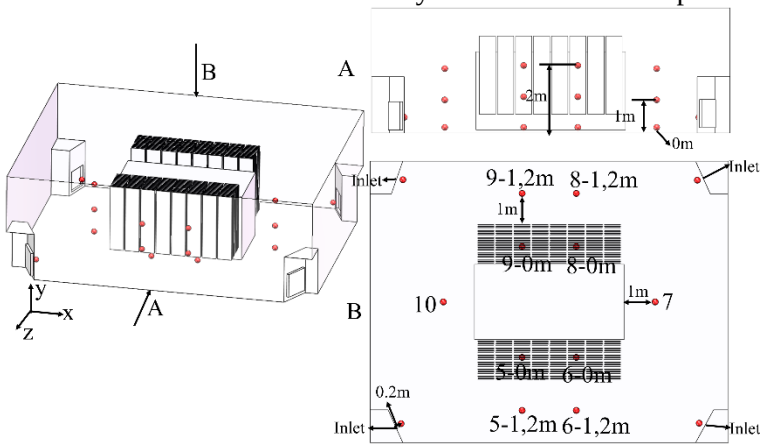

$$u_A(\bar{x}) = \sqrt{\frac{\sum_{i=1}^{n}(x_i - \bar{x})^2}{n(n-1)}} \quad (7)$$

$$\text{Error}_v = \frac{v_{simulation} - v_{test}}{v_{test}} \qquad \text{Error}_t = \frac{t_{simulation} - t_{test}}{t_{test}} \quad (8)$$

Fig. 4 Pictures of the spot test points

Tab.6 Test instrument introduction

PTS-XYZ Temperature sensor			Ultrasonic anemometer		
Picture	Fundamental characteristics	Parameter	Picture	Fundamental characteristics	Parameter
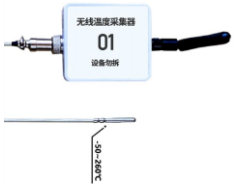	Measuring range	-200-550℃		Type	WQX2
	Measurement accuracy	±0.5℃		Measuring range	0-70m/s
	Operating ambient temperature	-40-80℃		Measuring accuracy	±0.1m/s

As can be seen from **Tab. 6**, the uncertainty of the temperature measuring instrument is ±0.5℃, and that of wind speed measuring instrument is ±0.1m/s. This is the uncertainty of the instruments themselves. The following is an analysis of the uncertainty of the measured quantity. The tests carried out in this paper are to measure the wind speed and temperature of the main transformer chamber, which are direct measurements. The Class A uncertainty is obtained by measuring the physical quantity x with the same precision for several times. The calculation formula is equation (8). In equation (8), x_i is measured quantity, $\bar{x}$ is the mean value and n is number of measurements. The test lasted 10 minutes and the instrument was able to collect data every 5s, so n refers to the amount of data. The uncertainty of wind speed and temperature at each measuring point is shown in **Tab. 7**. The uncertainty of temperature and wind speed at each measuring point is in reasonable context, so the test has better accuracy.

Tab.7 Class A uncertainty of test points

Test point	$u_A(v)$			$u_A(t)$		
	0m	1m	2m	0m	1m	2m
5	0.0116	0.0085	0.0083	0.0102	0.0153	0.0113
6	0.0276	0.0093	0.0085	0.0117	0.0131	0.0075
7	0.0245	0.0128	0.0081	0.0104	0.0184	0.0078
8	0.0099	0.0099	0.0054	0.01	0.0055	0.014
9	0.0108	0.004	0.0056	0.0074	0.0127	0.0079
10	0.0077	0.0042	0.0039	0.0097	0.0086	0.0134

Numerical simulation of this transformer chamber was conducted based on the its own structural dimensions, test data and above numerical method. The error analysis between the physical test values and the simulated values is shown in **Tab.6**. The relative error is used to evaluate the error between test and simulation. The calculation formula is shown in equation (9). From **Tab.6**, it can be seen that the accuracy of most of the measurement points can be controlled within the error range of ±10%. However, due to the influence of some wiring, piping and other equipment in the test chamber, the error of individual test points will be larger than others, but it can still be controlled within ±15%. Therefore, the above numerical simulation method can be adopted in this study. This is used to verify the accuracy of the simulation calculation method.

Tab.6 Test and simulation data summary

	Height (m)	Test point number	5	6	7	8	9	10
Temperature *t*	0	Experiment (°C)	38.6	39.7	37.4	36.9	37.8	39
		Simulation (°C)	41.7	40.1	42.5	36.4	38.4	39.4
		$Error_t$	-8.03%	-1.01%	-13.64%	1.36%	-1.59%	-1.03%
	1	Experiment (°C)	40.6	40.9	39.1	37.8	38.8	40.7
		Simulation (°C)	39.7	40.4	41.6	36.6	38.7	40.6
		$Error_t$	2.22%	1.22%	-6.39%	3.17%	0.26%	0.25%
	2	Experiment (°C)	41.1	42.7	39.5	39.3	40.3	42
		Simulation (°C)	42.7	40.9	41.9	39.1	40	41.4
		$Error_t$	2.68%	4.22%	-6.08%	0.51%	0.74%	1.43%
Wind speed *v*	0	Experiment (m/s)	0.87	0.5	0.62	0.65	0.82	0.67
		Simulation (m/s)	0.92	0.55	0.66	0.74	0.93	0.72
		$Error_v$	-5.75%	-10%	-6.45%	-13.85%	-13.41	-7.46%
	1	Experiment (m/s)	0.58	0.27	0.3	0.45	0.57	0.57
		Simulation (m/s)	0.61	0.28	0.28	0.46	0.56	0.62
		$Error_v$	-5.17%	-3.70%	6.67%	-2.22%	1.75%	-8.77%
	2	Experiment (m/s)	1.23	0.24	0.98	0.18	0.42	0.62
		Simulation (m/s)	1.17	0.23	0.99	0.17	0.45	0.44
		$Error_v$	4.88%	4.17%	-1.02%	5.56%	-7.14%	29.03%

5 Results and discussion

5.1The Influence of the location of the exhaust vent

In this section, the influence of different air outlet positions with three different air intake configurations on ventilation and heat dissipation performance is studied. **Section 5.1.1** investigates the effects of different outlet positions when the air inlet is parallel to the radiator plane (As shown in **Fig.2(a)**). **Section 5.1.2** investigates the effects of different outlet positions when the air inlet is perpendicular to the radiator plane (As shown in **Fig.2(b)**). **Section 5.1.3** investigates the influence of different outlet positions in the case of two opposite air inlets perpendicular to the radiator plane (As shown in **Fig.2(c)**).

5.1.1 Air inlet parallel to the radiator plane

This section studies the influence of the location of the exhaust outlet on the ventilation and heat dissipation performance of the main transformer chamber when the air inlet is located at the bottom of the side wall and parallel to the radiators (i.e., Scheme 1). According to the numerical simulation results, representative cross-sections were selected for analysis. The velocity distribution of different fan positions in the main transformer chamber at these cross-sections is shown in **Fig. 5**.

The same phenomenon that can be observed in these scenarios is that outdoor low-temperature air enters the main transformer chamber through a unilateral air inlet. The wind speed is higher in the radiator gap near the air inlet. When the chilly air encounters the main transformer, a portion of it sweeps outward to the sides of the main transformer, creating a low-speed vortex region near the sides. There is a high flow rate area in the middle and upper part of the main transformer chamber due to the suction effect of the fan on the indoor air. When the fans are located at the top of the main transformer chamber (Scenario A), the chilly air absorbs heat and rises. It is then discharged from the top of the transformer chamber due to the combined action of the floating lift force and the fans. When the fans are located on the same side as the inlet (Scenario B), the warm air flowing out from the radiators is affected by its inertia and the fans. As a result, the mainstream area of the warm air becomes curved. When the fans are adjacent to or opposite the air intake (Scenario C and Scenario D), the warm air is influenced by the edge of the natural ventilation well. Some of the warm air flows into the natural ventilation well and then back into the room. The placement of fans on the side wall of the main transformer chamber increases the flow path of the air, which leads to an increase in the residence time of the warm air in the room. This is not conducive to the ventilation of the main transformer chamber.

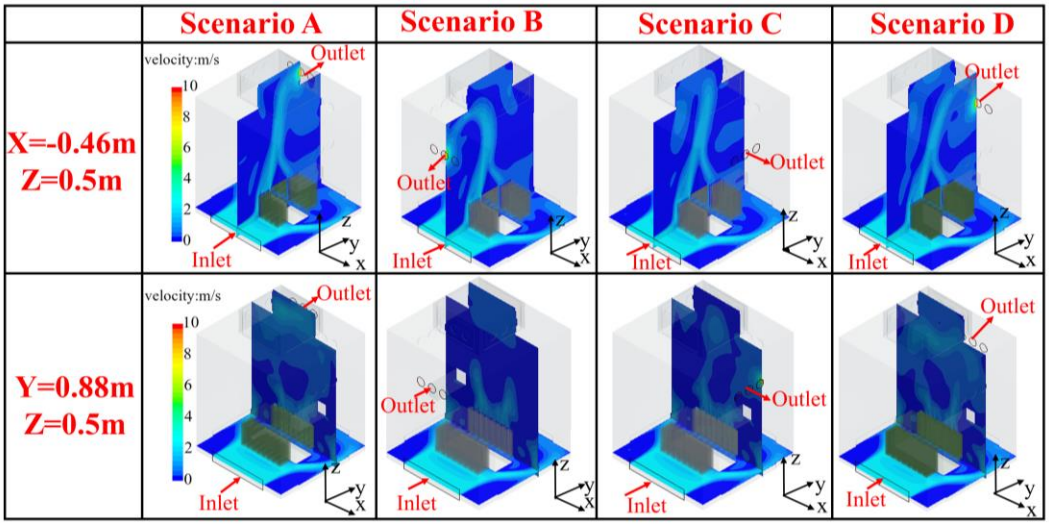

Fig. 5. Velocity distribution of the main transformer chamber when the inlet is parallel to the radiator plane

In **Fig.6**, the temperature distribution is shown for a cross-section perpendicular to the surface of the fan. The temperature of the radiator surface near the air inlet is lower compared to the other side. This is because a larger volume of chilly air flows into the radiator gap near the air inlet. On the outer edge of the radiators on this side, there is a low-temperature area. This is because the fans cause the air to be slightly scattered on the outside surface of the radiators, leading to heat exchange. The contact area between the air and the radiator surface is small, resulting in less rise in air temperature and underutilisation of the cooling capacity of the chilly air. As the height increases, the high-temperature air mixes with the remaining low-temperature air, causing the warm air temperature to decrease. The overall temperature distribution trend in the main transformer chamber is that the indoor air temperature increases with an increase in height. It can be observed from the image that the air temperature at the top of the main transformer room is high. In scenario A, the fan is located at the top of the main transformer room, which can discharge the warm air in time. In scenarios B, C, and D, the temperature near the fan is lower than the temperature at the top of the main transformer room, indicating that the fan does not remove the warm air in the room in time. when the fans are located at the top of the main transformer chamber, it has a lower indoor air temperature compared to the other three locations (B, C, and D). This indicates that when the fan is located on the side wall (scenarios B, C, and D), the fans are unable to discharge the indoor high-temperature air to the outside in time. As a result, high-temperature air accumulates on the top of the main transformer chamber, increasing the residence time of high-temperature air in the room. This is not conducive to the heat dissipation of the main transformer chamber.

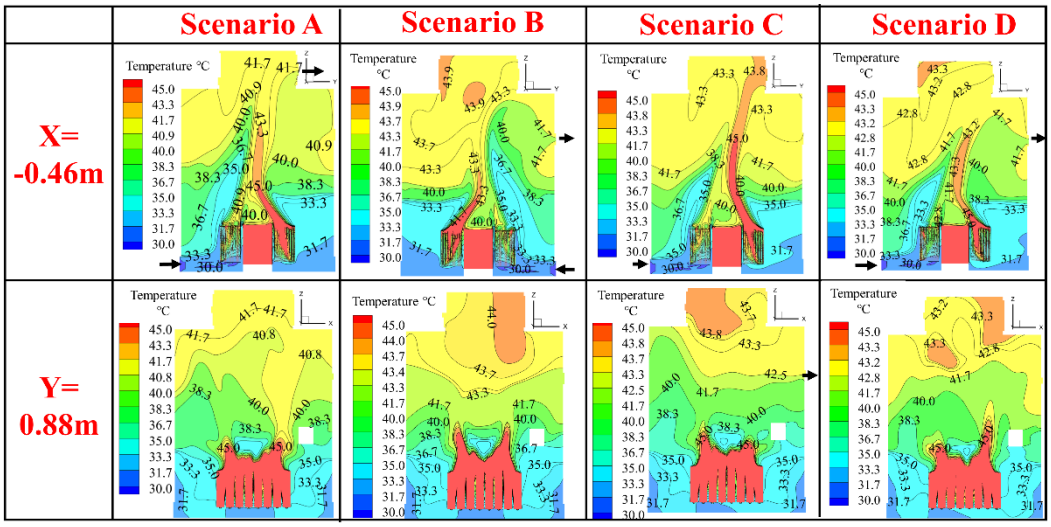

Fig.6. Temperature distribution of the main transformer chamber when the inlet is parallel to the radiator plane

In this paper, the energy utilisation coefficient [24-26] is introduced to evaluate the ventilation and heat dissipation effects of indoor substations. The calculation formula is as follows:

$$\eta = \frac{t_{out} - t_{in}}{t_a - t_{in}} \tag{9}$$

where t_{in} is the inlet temperature, ℃; t_{out} is the outlet temperature, ℃; t_a is the average air temperature in the main transformer chamber, ℃. A larger energy utilisation coefficient indicates better ventilation and heat dissipation performance.

The surface heat transfer coefficient represents the efficiency of heat transfer between the heat transfer medium and the heat transfer surface. The calculation formula is as follows:

$$h = \frac{Q}{A\Delta t} \tag{10}$$

where Q is the heat exchange capacity, W; h is the surface transfer coefficient, $W \cdot m^{-2} \cdot K$; A is the heat transfer area, m^2; Δt is the temperature difference between the air and the solid surface. Here, h_t represents the surface heat transfer coefficient of the main transformer and h_r represents the surface heat transfer coefficient of the radiators.

Fig.7 shows the changes in the maximum temperature of the main transformer (T_{max}), energy utilisation coefficient (η), and convective heat transfer coefficient of the main transformer (h_t) and the radiators (h_r) with the position of the exhaust fans. It indicates that when the exhaust fans are placed at the top of the main transformer chamber (Scenario A), the warm air inside the room can be effectively expelled, resulting in a lower indoor air temperature. The lowest temperature recorded for the main transformer is 81.7°C when the fans are located at the top of the main transformer chamber. The energy utilisation coefficient is the highest at 1.38 when the fans are placed at the top. When comparing the results with other fan locations, it is observed that placing the fans at the top of the main transformer chamber leads to a maximum decrease in the temperature of the main transformer by 0.5°C. Additionally, the energy utilisation coefficient increases by 10.4% maximally. When the fans are placed at the top, both the main transformer and the chip radiators experience an improvement in their convective heat transfer coefficients. The convective heat transfer coefficient for the main transformer maximally increases by

5.6% to 6.01W·m^{-2}·K^{-1}, while for the chip radiators, it maximally increases by up to 6.4% to 4.17 W·m^{-2}·K^{-1}.

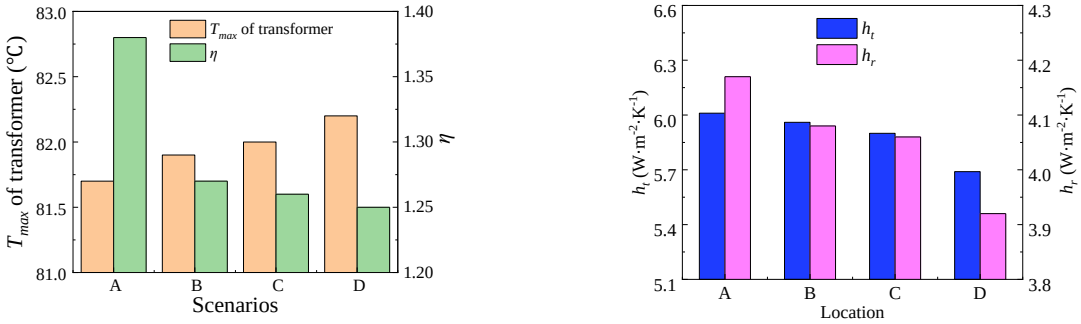

Fig. 7. Comparison of parameters under different fan positions

5.1.2 Air inlet perpendicular to the radiator plane

This section studies the influence of the location of the exhaust outlet on the ventilation and heat dissipation of the main transformer chamber when the air inlet is located at the bottom of the side wall perpendicular to the radiator (Scheme 2).

Different cross-sections of the main transformer chamber were selected for analysis. **Fig. 8** shows the distribution of air velocity in these different areas. Chilly air enters the main transformer chamber through the air inlet. The chilly air encounters the main transformer and splits into two parts. These two parts of air flow towards the radiators located on both sides of the transformer. The air enters the gap between the radiators to exchange heat with them. As the chilly air moves towards the opposite side of the air inlet, a significant amount of air flows upward. This upward flow causes the high-velocity area to become narrower over time. Because the airflow tends to flow in the -X and +Z directions, the airflow above the radiator is inclined. Additionally, two small vortices are formed on the side of the main transformer far away from inlet. If the fans are positioned at the top of the main transformer chamber (Scenario A), the warm air, which has exchanged heat with the radiators, rises to the top of the room. The fans are then able to expel the warm air from the main transformer chamber. If the fans and the air inlet are on the same side (Scenario B) and adjacent to the inlet (Scenario C), the warm air flows towards the top of the main transformer chamber. However, this flow is affected by the corner of the natural ventilation shaft, causing the air to divide into two parts. Most of the air flows to the top of the main transformer chamber and is then expelled by the fans, which increases the flow path. A small portion of the air forms a vortex near the wall, causing the warm air to stay in the room for a longer time. When the fan is opposite the air inlet (Scenario D), due to the influence of the edge of the wall above the fan, part of the hot air returns to the main transformer chamber, and it cannot be excluded from the main transformer chamber. The velocity of the air at the top of the main transformer chamber is high in Scenarios B, C and D, indicating that some of the warm air does not directly leave through the fans but instead flows through the top of the room before being expelled. This leads to an increase in the flow path of the warm air and the accumulation of heat at the top of the main transformer chamber, which hinders the rapid discharge of warm air from the room.

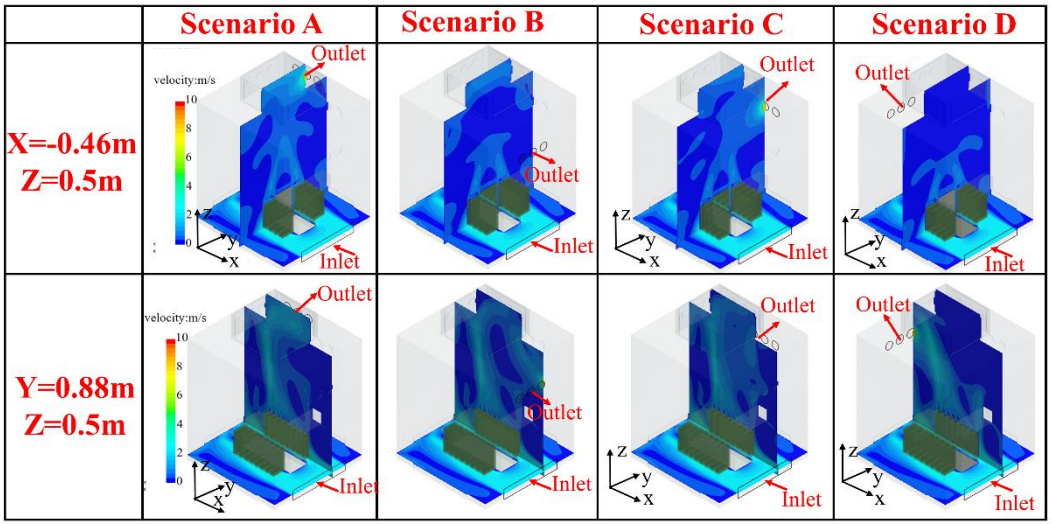

Fig. 8. Velocity distribution of the main transformer chamber when the inlet is perpendicular to the radiator plane

The temperature distribution was visualized in **Fig.9**. When the chilly air enters the room, it comes into contact with the radiators, which are responsible for dissipating heat from the transformer. As the chilly air exchanges heat with the radiators, its temperature increases. As the air flows upwards in the room, carrying the heat from the radiators, the temperature above the radiators becomes high. This is because the air is in direct contact with the hot radiators and absorbs the heat from them. As the high-temperature air flows upwards and interacts with the cooler indoor air, there is a slight decrease in temperature. However, the overall trend is that as the height increases, the air temperature also increases. This means that the upper regions of the main transformer chamber tend to have higher temperatures compared to the lower regions. It is found that the air temperature at the air inlet is lower. When the radiator is closer to the inlet, it has a better cooling effect because it exchanges heat with the air with a lower temperature. when the fans are located at the top of the room (Scenario A), the overall temperature in the room is lower compared to the other three positions (Scenarios B, C, D). It can be observed from the image that the air temperature at the top of the main transformer room is high. In scenario A, the fan is located at the top of the main transformer room, which can discharge the warm air in time. In scenarios B, C, and D, the temperature near the fan is lower than the temperature at the top of the main transformer room, indicating that the fan does not remove the warm air in the room in time. This indicates that the fans are not able to effectively remove the high-temperature air from the room, leading to the accumulation of warm air at the top of the room, which is not ideal for ventilation and heat dissipation in the main transformer chamber.

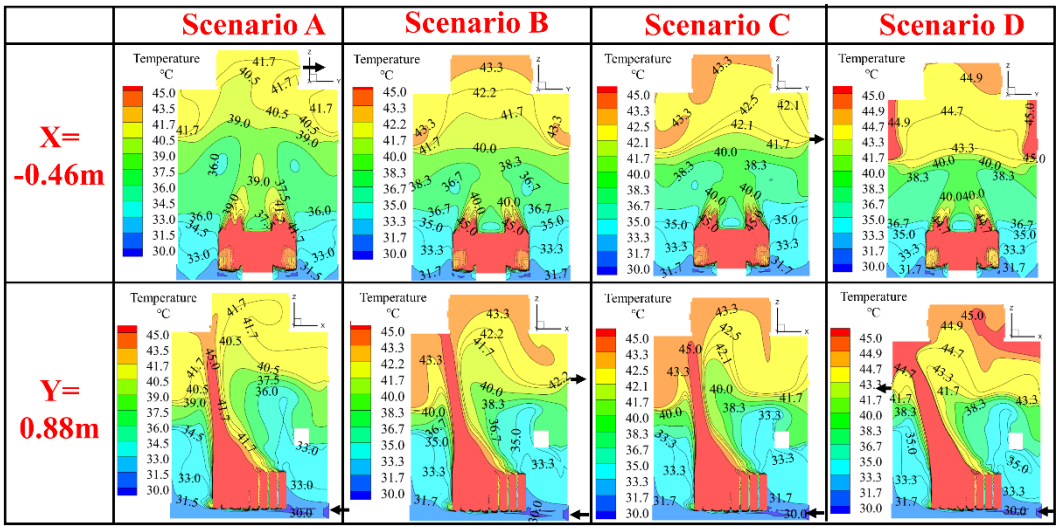

Fig. 9. Temperature distribution of the main transformer chamber when the inlet is perpendicular to the radiator plane

Fig.10 shows a comparison of parameters related to different fan positions. When the fans are placed at the top of the main transformer chamber (Scenario A), the temperature of the main transformer is the lowest at 80.6°C and the energy utilisation coefficient is the highest at 1.52. Compared to other air outlet positions, placing the fans at the top of the main transformer chamber (Scenario A) results in a maximum reduction of 0.8°C in the temperature and a maximum increase of 18.8% in the energy utilisation coefficient. When the fans are placed at the top of the main transformer chamber (Scenario A), both the main transformer and chip radiator have the highest surface heat transfer coefficient. The surface heat transfer coefficient for the main transformer is 5.44 $W \cdot m^{-2} \cdot K^{-1}$, and for the chip radiator, it is 4.41 $W \cdot m^{-2} \cdot K^{-1}$. Compared to other scenarios, there is a maximum improvement of 2.1% in the surface heat transfer coefficient for the main transformer and 2.3% for the chip radiator.

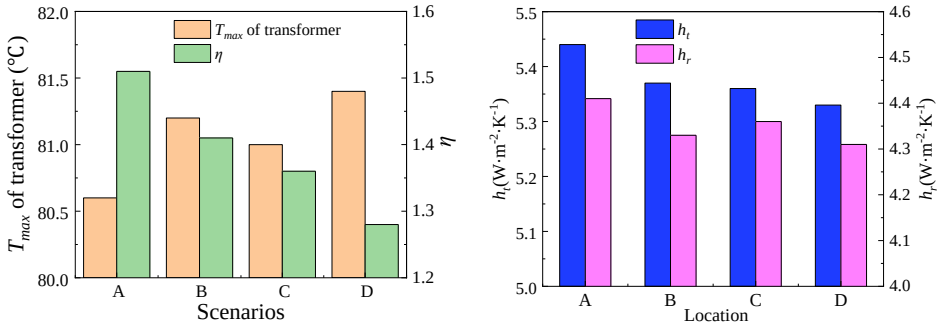

Fig. 10. Comparison of parameters under different fan positions

5.1.3 Two opposite air inlets perpendicular to the radiator plane

This section studies the influence of the location of the exhaust outlet on the ventilation and heat dissipation of the main transformer chamber when the air inlet is located at the bottom of the side wall perpendicular to the radiator (Scheme 3).

To compare the velocity distributions for four different fan positions, the results are visualized in **Fig. 11**. The same phenomenon that can be observed is that the air flows to the transformer and is divided into two equal parts. Two opposite flows of air create a hedge. This enhances the disturbance and helps to

dissipate heat. When the fans are located on the top of the main transformer (Scenario A), the airflow speed above the main transformer is higher, and the high-velocity area in the main transformer chamber is concentrated in the middle area between the top of the main transformer chamber and the top of the main transformer. The air flows upward in a straight line under the combined action of the floating lift and the fan, and the flow path is short. However, when the fan is located on the side wall (Scenarios B, C and D), the flow state of the air in the upper part of the main transformer chamber is changed. What can be seen is that the top airflow velocity is higher because it first flows to the top of the main transformer chamber and then flows out of the exhaust outlet. This increases the flow path of the air and causes high temperature air is not easy to discharge the main transformer chamber, resulting in heat accumulation at the top, which is not conducive to heat dissipation.

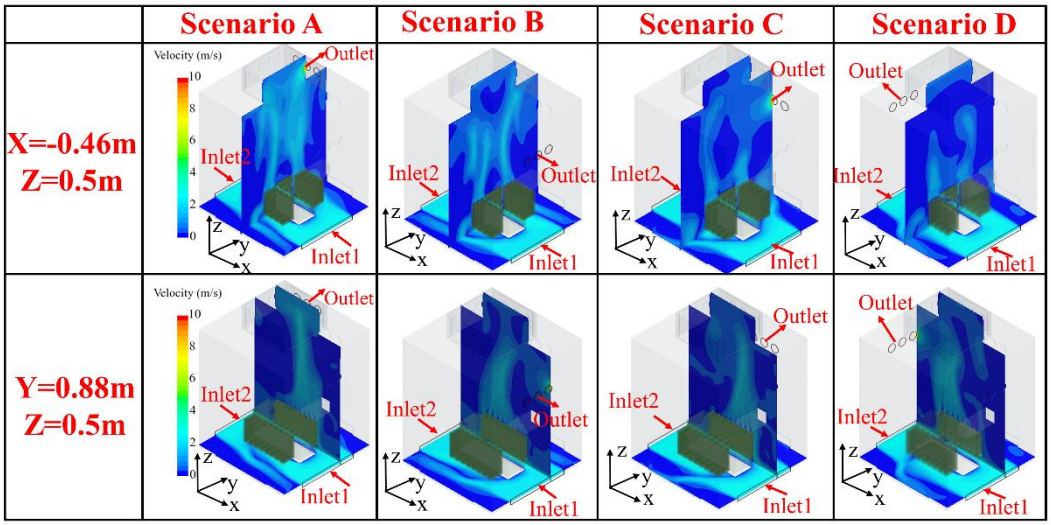

Fig. 11. Velocity distribution of the main transformer chamber when the two opposite inlets are perpendicular to the radiator plane

Fig. 12 represents the temperature distribution in the main transformer chamber under different conditions. In these four cases, low-temperature air enters the transformer chamber through two inlets. This low-temperature air then flows into the gap between the radiator and the cooling fins. The purpose of this flow is to exchange heat with the cooling fins and dissipate the heat generated by the transformer. As the low-temperature air flows above the main transformer chamber, its temperature rises. This is because the low-temperature air mixes with the warm air generated by the transformer and the cooling fins. The warm air flowing upward from the transformer chamber mixes with the indoor low-temperature air, causing the temperature of the warm air to decrease. Due to the mixing of hot and low-temperature air, the high-temperature area in the main transformer chamber is concentrated near the main transformer and the radiators. The indoor temperature distribution in the main transformer chamber is shown in **Fig.13**. The temperature in the main transformer chamber shows a stratification phenomenon, meaning that the temperature gradually increases from the bottom to the top of the room. It is observed that when the fan is located at the top of the main transformer chamber (Scenario A), the air temperature above the main transformer is higher. This indicates that the heat carried away by the air is greater, resulting in better cooling of the transformer. On the other hand, when the fan is located on the side wall (Scenarios B, C and D), the temperature at the top of the main transformer chamber is higher than that at the fan outlet,

indicating that the fan does not discharge the high-temperature air in the main transformer chamber, resulting in the accumulation of hot air at the top of the main transformer chamber.

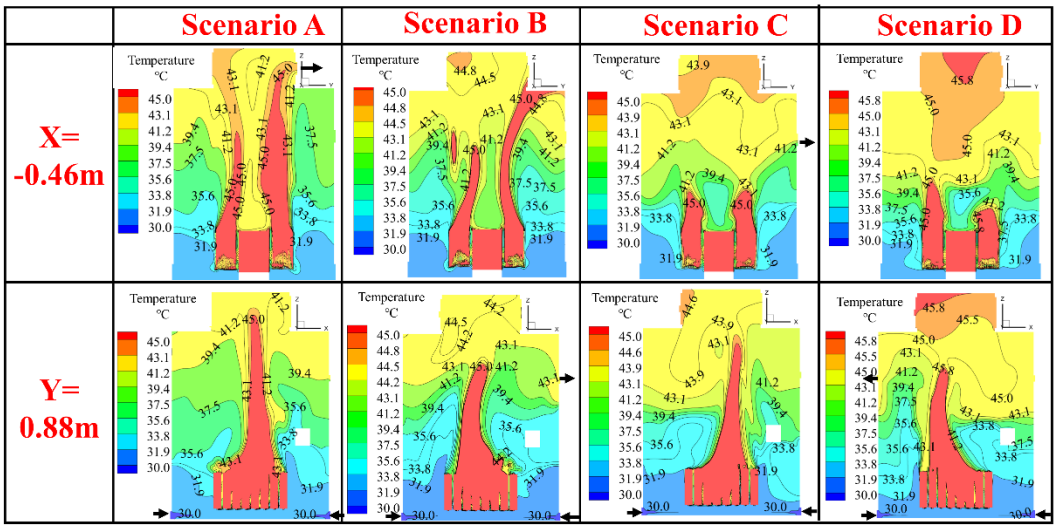

Fig.12. Temperature distribution of the main transformer chamber when the two opposite inlets are perpendicular to the radiator plane

According to **Fig.13**, when the fan is located at the top of the main transformer (Scenario A), the energy utilisation coefficient increases by up to 24.8% compared to when the fan is located at another location. This means that when the fan is placed at the top, the cooling air is used more efficiently for heat dissipation in the room. As a result, the maximum temperature of the main transformer is reduced by up to 1.6°C compared to when the fan is located at another location. This temperature reduction is significant as it helps in maintaining the stability and proper functioning of the transformer. Additionally, the heat transfer coefficient between the main transformer and the sheet scatter surface increases by up to 4.5% and 2.5%, respectively. This indicates that the heat transfer process becomes more effective, allowing for better dissipation of heat from the main transformer to the surrounding environment.

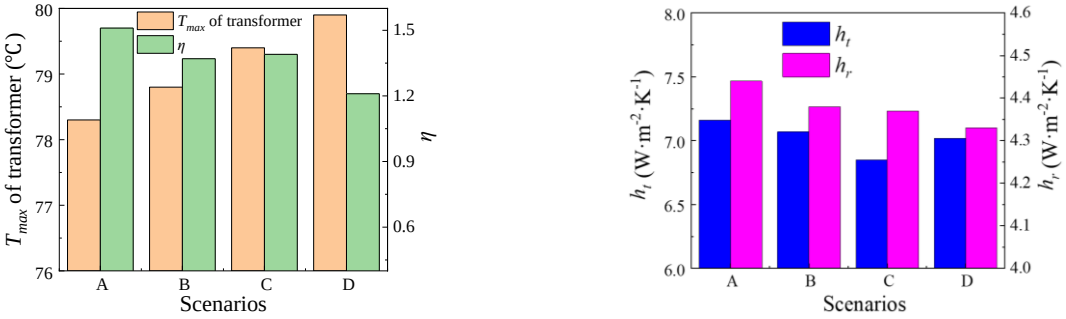

Fig.13. Comparison of parameters of various positions of exhaust vents

5.2 Effect of the inlet position

According to the research results in **5.1.1**, **5.1.2** and **5.1.3**, regardless of where the intake is located, the effect of ventilation and heat dissipation is best when the exhaust is located at the top of the main transformer chamber. Therefore, this section compares the influence of various positions of the air inlet on the ventilation and heat dissipation of the main transformer chamber when the exhaust outlet is located at the top of the main transformer chamber, at the same time, keep the total area of the air inlet unchanged,

only change the position of the air inlet, as shown in **Fig. 14**.

In Scheme 1, the air inlet is located at the central bottom of the wall parallel to the plane where the radiators are located. This arrangement allows a large amount of air to flow into the radiator gap that is close to the air inlet. Additionally, because the length of the air inlet is longer than the length of the main transformer, a small amount of cooling air flows from the side of the main transformer and is collected in the radiators far away from the air inlet. As a result, the volume of air on both sides of the main transformer is different, and the cooling wind speed between the radiators on both sides is different. In **Fig.14**, the air velocity between the radiators closer to the inlet is larger, indicating better cooling effect of those radiators. In Scheme 2, the air inlet is located at the central bottom of the wall perpendicular to the plane where the radiators are located. The length of the air inlet is greater than the distance between the two sides of the radiators. As a result, the air is divided into two average parts after meeting the main transformer and flows to the two sides of the radiators. **Fig. 14** shows that there is no difference in the flow rate between the radiators on both sides of the transformer, indicating that the airflow into the radiators is equal, ensuring uniform cooling. However, the air density decreases due to the increase of the flow channel and the increase of the air temperature after heat exchange with the heat sink. The air flows above the main transformer chamber under the action of the fan and the floating lift. So the further away from the air inlet, the smaller the air velocity in the radiator. In Scheme 3, the air inlet is located at the central bottom of the two opposite walls perpendicular to the plane where the radiators are located. **Fig. 14** shows that the air flows into the main transformer chamber from both sides, overcoming the shortcomings of the previous two schemes. The wind speed difference between the radiators on both sides of the main transformer is small, and the air volume is evenly distributed, indicating that the radiators on both sides are evenly cooled. Additionally, due to the simultaneous intake of air on both sides, the air velocity does not decay along the flow direction, resulting in stable air velocity between the entire radiators.

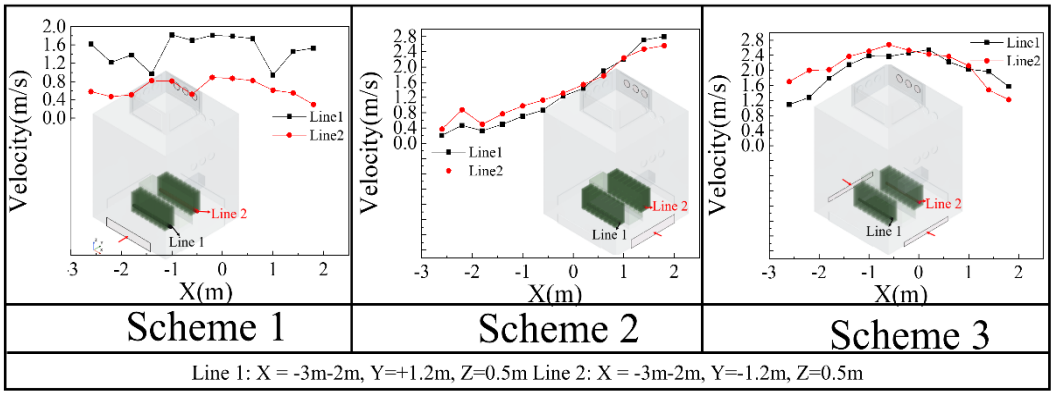

Fig.14. Variation in air velocity between radiators in three schemes

Fig. 15 shows a comparison of the positions of different air inlet schemes when the outlets are located at the top of the main transformer chamber. When the air inlet arrangement scheme is Scheme 3, the maximum temperature of the main transformer can be reduced by 3.4℃, and the energy utilisation coefficient can be increased by 9.4% compared to Scheme 1. The surface heat transfer coefficients of the main transformer and radiators can be increased by 31.6% and 6.5%, respectively.

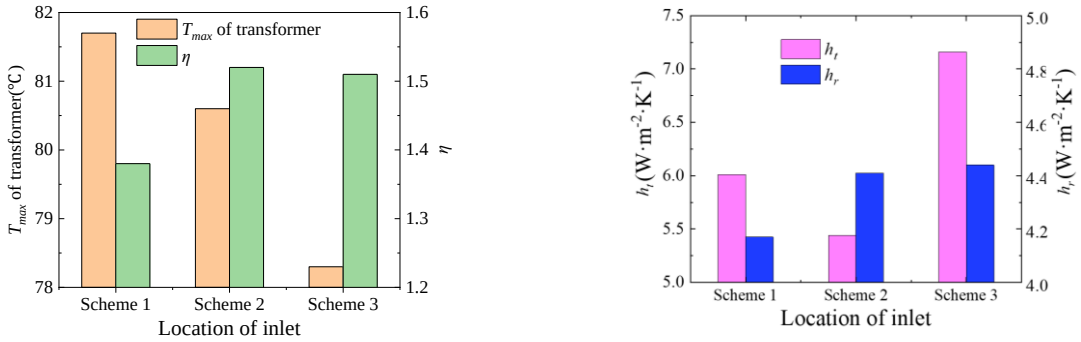

Fig. 15. Comparison of the positions of different air inlets

Under the condition of mechanical ventilation, the effect of optimising the position of the inlet is more obvious than that of optimising the position of the outlet. If the position of the air inlet remains constant and only the position of the exhaust outlet is changed, the maximum temperature of the main transformer is only reduced by a small amount, specifically between 0.5-1.1°C, on the other hand, if the position of the exhaust outlet remains the same and only the position of the air inlet is changed, the maximum temperature of the main transformer is reduced by a larger amount, specifically by 3.4°C. The air inlet is located near the main transformer and radiators, which are components that generate heat. The proximity of the air inlet to these heat-generating components affects the flow of air around them, leading to better heat dissipation and lower temperatures.

Based on the findings mentioned earlier, an optimal configuration for the ventilation system in the main transformer chamber is suggested. The fans should be positioned at the top of the main transformer chamber. The air inlets should be located at the central bottom of the two opposite walls of the main transformer chamber. These air intakes should be perpendicular to the plane where the radiators are located. By following this configuration, the main transformer chamber will have the best ventilation performance, resulting in lower temperatures and improved heat dissipation.

6 Conclusion

The paper constructs a numerical simulation model to study the ventilation and heat dissipation performance of an indoor substation under mechanical ventilation. The model is verified to ensure its accuracy and reliability. The study investigates how various positions of air intake and outlet affect the ventilation and heat dissipation performance of the main variable room.

(1) Regardless of the air intake position, when the fan is placed at the top of the main transformer chamber (Scenario A), it shortens the airflow path and facilitates the discharge of high-temperature air. This arrangement effectively reduces the accumulation of warm air, lowers the indoor air temperature, and decreases the maximum temperature of the transformer by 0.5-1.6°C. Additionally, it increases the energy utilisation coefficient by 8.6%-24.8%.

(2) The study explores different air inlet positions and finds that when the air inlet is located at the bottom of the two side walls perpendicular to the radiator (Scheme 3), it ensures an even distribution of wind speed between the two sides of the blade scatter. This allows for maximum utilisation of cooling wind, leading to a reduction of the maximum temperature of the main transformer by 3.4°C. Furthermore, it increases the energy utilisation coefficient by 9.4% and improves the heat transfer area and coefficient.

(3) Comparing the influence of inlet and outlet positions, the study finds that optimizing the inlet position has a greater effect on indoor ventilation and heat dissipation performance compared to the outlet position. This indicates that the inlet position has a more significant impact on the overall performance of the system. Therefore, in practical projects, priority should be given to optimizing and transforming the inlet position.

Nomenclature

A	The heat transfer area (m^2)
h	Surface heat transfer coefficient ($W \cdot m^{-2} \cdot K^{-1}$)
h_t	Surface heat transfer coefficient of the main transformer ($W \cdot m^{-2} \cdot K^{-1}$)
h_r	Surface heat transfer coefficient of the radiators ($W \cdot m^{-2} \cdot K^{-1}$)
Q	The heat exchange capacity (W)
t_{in}	Temperature of inlet (℃)
t_{out}	Temperature of outlet (℃)
t_a	Volume mean temperature of air in the main transformer chamber (℃)
T_{max}	The maximum temperature of the main transformer (℃)
η	Energy utilisation coefficient

Acknowledgement

The present work is supported by the National Natural Science Foundation of China (No.52276019).

Reference

[1] Xie, R., *et al*., Optimization of Ventilation and Heat Dissipation Structure of Transformer Chamber in Prefabricated Substation Based on Multi-Physics Coupling, *2023 IEEE 4th International Conference on Electrical Materials and Power Equipment (ICEMPE)*, Shanghai, China, 2023, pp.1-3

[2] Liu, Y., *et al*., Ventilation Optimization for Reduction of Indoor Air Temperature of Main Transformer chamber in Urban Indoor Substation by the Variational Method, *Journal of Thermal Science*,*28*(2019),5, pp.1089-1101.

[3] Xu, L., *et al*., A Fast Computational Fluid Dynamics Model for the Flow and Heat Transfer Characteristics Analysis of Indoor Substation Rooms, *IOP Conference Series: Materials Science and Engineering*, *199*(2017), 1, 012076.

[4] Liu, H., *et al*. Study on ventilation of indoor substation main transformer chamber based on COMSOL software, *International Conference on Electrical Materials and Power Equipment (ICEMPE)*, Xi'an, China, 2017, pp.296-300.

[5] Xu R., et al., Simulation Study on Ventilation & Cooling for an Indoor Substation, *Applied Mechanics and Materials*,*672*(2014), pp.672-674.

[6] Cheng, L., *et al*., Influence of Box-in Structure on Heat Dissipation Performance of UHV Converter Transformer, *2021 IEEE 4th International Electrical and Energy Conference (CIEEC)*, Wuhan, China, 2021, pp.1-6.

[7] Wei, B., *et al*., Study on simulation test device of transformer split type cooling system, *Energy Procedia*, *100* (2016), pp. 556-560.

[8] Niu, W., *et al*. The experimental study of a novel cooling system of a power transformer in an urban underground substation,2010 International Conference on Power System Technology. IEEE, 2010, pp.1-6.
[9] Peng, L., *et al*., Numerical Analysis of Temperature Field of Outdoor Transformer with Noise Barrier, *Journal of Physics: Conference Series*,*1600*(2020),1,012056.
[10] Perng, J. W., *et al*., Power Substation Construction and Ventilation System Co-Designed Using Particle Swarm Optimization, *Energies*, *13*(2020), 2314.
[11] Wiriyasart, S., *et al*., Numerical study on air ventilation in the workshop room with multiple heat sources, *Case Studies in Thermal Engineering*,*13* (2019), 100405.
[12] Zheng, C., *et al*., Comparison of air-conditioning systems with bottom-supply and side-supply modes in a typical office room, *Applied Energy*, *227* (2018), pp.304-311.
[13] Chen, H., *et al*., Numerical investigation of ventilation performance of different air supply devices in an office environment, *Building and Environment*, *90* (2015), pp.37-50.
[14] Chen Y., et al., Study of ventilation cooling technology for telecommunication base stations in Guangzhou, *Energy & Buildings*, *41*(2009),7, pp.738-744.
[15] He, Y., *et al*., Experimental and CFD study of ventilation performance enhanced by roof window and mechanical ventilation system with different design strategies, *Building and Environment*, 224(2022),109566.
[16] Tong, L., *et al*., A novel flow-guide device for uniform exhaust in a central air exhaust ventilation system, *Building and Environment*, *149*(2019), pp.134-145.
[17] Staveckis, A., *et al*., Impact of impinging jet ventilation on thermal comfort and indoor air quality in office buildings, *Energy and Buildings*, *235*(2021), 110738.
[18] Huang, Y., *et al*., Effects of the ventilation duct arrangement and duct geometry on ventilation performance in a subway tunnel, *Tunnelling and Underground Space Technology*, *26*(2011), 6, pp. 25-733.
[19] Huang, Y., et al., A numerical analysis of the ventilation performance for different ventilation strategies in a subway tunnel, *Journal of Hydrodynamics*, Ser. B, *24*(2012),2, pp.193-201.
[20] Park, J., *et al*. CFD modelling of ventilation ducts for improvement of air quality in closed mines, *Geosystem Engineering*, *19*(2016), 4, pp.177-187.
[21] Panchal, S., *et al*. Numerical simulation of cooling plate using K-epsilon turbulence model to cool down large-sized graphite/LiFePO4 battery at high C-rates, *World Electric Vehicle Journal*, *13*(2022),8, pp.138.
[22] Li, J., *et al*. Coarse-grid simulations of full-loop gas-solid flows using a hybrid drag model: Investigations on turbulence models, *Powder Technology*, *379*(2021), pp.108-126.
[23] ***, Tutorials of the STAR-CCM+2206, https://www.sw.siemens.com.
[24] Li, H., *et al*., Study on the impact of parallel jet spacing on the performance of multi-jet stratum ventilation, *Applied Energy*, *306*(2022), 118135.
[25] Karimipanah, T., *et al*., Investigation of air quality, comfort parameters and effectiveness for two floor-level air supply systems in classrooms, *Building and Environment*, *42*(2007), 2, pp.647-655.
[26] Gao, R., *et al*., A new evaluation indicator of air distribution in buildings, *Sustainable Cities and Society*, *53* (2020), 101836.

Paper submitted: 06.02.2024
Paper revised: 18.03.2024
Paper accepted: 25.03.2024